# Phosphorylation of KLC1 modifies interaction with JIP1 and abolishes the enhanced fast velocity of APP transport by kinesin-1

Kyoko Chiba[a], Ko-yi Chien[b], Yuriko Sobu[a], Saori Hata[a], Shun Kato[a], Tadashi Nakaya[a], Yasushi Okada[c,d], Angus C. Nairn[e], Masataka Kinjo[f], Hidenori Taru[a], Rong Wang[b], and Toshiharu Suzuki[a,*]

[a]Laboratory of Neuroscience, Graduate School of Pharmaceutical Sciences, Hokkaido University, Sapporo 060-0812, Japan; [b]Department of Genetics and Genomic Sciences, Icahn School of Medicine at Mount Sinai, New York, NY 10029; [c]Laboratory for Cell Polarity Regulation, RIKEN Quantitative Biology Center, Suita 565-0874, Japan; [d]Department of Physics, Graduate School of Science, University of Tokyo, Tokyo 113-0033, Japan; [e]Department of Psychiatry, Yale University School of Medicine, New Haven, CT 06508; [f]Laboratory of Molecular Cell Dynamics, Faculty of Advanced Life Science, Hokkaido University, Sapporo 001-0021, Japan

**ABSTRACT** **In neurons, amyloid β-protein precursor (APP) is transported by binding to kinesin-1, mediated by JNK-interacting protein 1b (JIP1b), which generates the enhanced fast velocity (EFV) and efficient high frequency (EHF) of APP anterograde transport. Previously, we showed that EFV requires conventional interaction between the JIP1b C-terminal region and the kinesin light chain 1 (KLC1) tetratricopeptide repeat, whereas EHF requires a novel interaction between the central region of JIP1b and the coiled-coil domain of KLC1. We found that phosphorylatable Thr466 of KLC1 regulates the conventional interaction with JIP1b. Substitution of Glu for Thr466 abolished this interaction and EFV, but did not impair the novel interaction responsible for EHF. Phosphorylation of KLC1 at Thr466 increased in aged brains, and JIP1 binding to kinesin-1 decreased, suggesting that APP transport is impaired by aging. We conclude that phosphorylation of KLC1 at Thr466 regulates the velocity of transport of APP by kinesin-1 by modulating its interaction with JIP1b.**

**Monitoring Editor**
Kozo Kaibuchi
Nagoya University

Received: May 17, 2017
Revised: Sep 18, 2017
Accepted: Oct 26, 2017

## INTRODUCTION

Amyloid β-protein precursor (APP), a type I membrane protein that is processed to form amyloid β-protein (Aβ), is deeply implicated in Alzheimer's disease pathogenesis. The APP gene generates three main isoforms: APP695, APP750, and APP770. Although APP is ubiquitously expressed in many tissues, APP695 is expressed exclusively and at high levels in neurons (reviewed in Suzuki and Nakaya, 2008; Huang and Mucke, 2012).

One of the most important functions of APP in neurons is as a cargo receptor for kinesin-1, a conventional kinesin, which was first identified as an anterograde molecular motor in squid giant axon (Vale *et al.*, 1985). Functional kinesin-1 forms a tetramer comprising two kinesin heavy chains (KHCs) and two kinesin light chains (KLCs), and plays an essential role in anterograde transport of many cargoes, including membrane vesicles, organelles, and RNA. This transport function is especially critical in neurons, which form huge numbers of connections with each other via extended neurites (reviewed in Hirokawa *et al.*, 2010; Bentley and Banker, 2016). Kinesin-1 is the most extensively analyzed anterograde motor of the kinesin superfamily of proteins (KIFs); accordingly, many of its biophysical properties, including generation of mechanical force driven by ATP hydrolysis, are well understood (reviewed in Lu and Gelfand, 2017). Furthermore, several recent studies have demonstrated the importance of

This article was published online ahead of print in MBoC in Press (http://www.molbiolcell.org/cgi/doi/10.1091/mbc.E17-05-0303) on November 1, 2017.

*Address correspondence to: Toshiharu Suzuki (tsuzuki@pharm.hokudai.ac.jp).

Abbreviations used: AD, Alzheimer's disease; APP, amyloid β-protein precursor; CAD, mouse CNS catecholaminergic cell line; EFV, enhanced fast velocity; EHF, efficient high frequency; GFP, green fluorescent protein; JIP1, JNK-interacting protein 1; JNK, c-Jun $NH_2$-terminal kinase; KHC, kinesin heavy chain; KLC, kinesin light chain; N2a, mouse neuroblastoma Neuro-2a cells; TPR, tetratricopeptide repeat.

adaptor proteins for effective transport of cargo by kinesin-1 and activation of auto-inhibited motors (Verhey *et al.*, 2001; Verhey and Hammond 2009; Kawano *et al.*, 2012; Chiba *et al.*, 2014a; Yip *et al.*, 2016).

In contrast to the motor functions of kinesin-1, we understand far less about the components of cargoes transported by kinesin-1 and the roles of cargo receptors, which are membrane proteins functionally connected to kinesin-1 either directly or indirectly via adaptor proteins. The JNK-binding proteins (JIPs; JIP1, JIP2, and JIP3), originally identified as scaffold proteins of the JNK signaling cascade (Dickens *et al.*, 1997), have been identified as adaptors that connect cargo receptors to kinesin-1 (Scheinfeld *et al.*, 2002; Taru *et al.*, 2002). JIP1 mediates interactions between kinesin-1 and cargo receptors such as APP and apolipoprotein E receptor (APOER) (Verhey *et al.* 2001). In addition to connecting cargo receptors to kinesin-1, JIP1 also modulates cargo transport. Binding of JIP1 to KHC activates kinesin-1, promoting processivity, and also coordinates anterograde and retrograde transport by modulating association of vesicles with dynein, a retrograde molecular motor (Fu and Holzbaur, 2013).

Furthermore, the interaction between JIP1b and KLC1 is essential for efficient anterograde axonal transport of APP cargo, including enhanced fast velocity (EFV) and efficient high frequency (EHF) (Chiba *et al.*, 2014a). EFV of APP anterograde transport is accomplished via conventional interaction between the JIP1b 11-amino acid C-terminal region (C11) and the tetratricopeptide repeat (TPR) region of KLC1. Therefore, in anterograde transport, APP cargoes connected to kinesin-1 via JIP1b move much faster than, for example, Alcadeinα (Alcα) cargoes bound directly to kinesin-1 in vivo or kinesin-1 on microtubules in vitro (Kawaguchi and Ishiwata, 2000; Araki *et al.*, 2007; Chiba *et al.*, 2014a). EHF requires a novel interaction between the central region of JIP1b and the coiled-coil domain of KLC1, which contributes to the stable and higher-frequency anterograde transport of APP (Chiba *et al.*, 2014a). Although it remains unclear how the interaction of JIP1b with kinesin-1 is selectively regulated to control APP cargo transport, it is obvious that temporally and regionally regulated binding of cargoes and/or adaptor proteins to kinesin-1 is required for efficient transport (Verhey *et al.*, 2001; Fu and Holzbaur, 2013).

Previous studies suggested that phosphorylation of components of cargo–motor complexes is involved in regulation of cargo transport. For example, phosphorylation of KLC2 influences binding of vesicular cargo to kinesin-1 (Morfini *et al.*, 2002). Phosphorylation of KLC1 at Ser460 specifically decreases binding of calsyntenin-1/Alcα (Vagnoni *et al.*, 2011), whereas phosphorylation of Alcα at multiple seryl residues is required for its interaction with the KLC of kinesin-1 (Sobu *et al.*, 2017). Activation of kinesin-1 by association of JIP1 with the KHC may also be modulated by phosphorylation of JIP1 by JNK (Fu and Holzbaur, 2013). However, little is known about the mechanism that regulates the interaction between JIP1 and KLC, notwithstanding the importance of this interaction for efficient transport of APP cargo by kinesin-1 (Chiba *et al.*, 2014a).

In this study, we found that phosphorylation of Thr466 of KLC1 regulates the interaction between KLC1 and JIP1b. Replacement of this residue with Glu to mimic phosphorylation abolished the conventional interaction between JIP1 and KLC1, resulting in reduction of the EFV of APP cargo transport mediated by JIP1b. Our findings suggest that posttranslational modification of a molecular motor can regulate the velocity of cargo transport by altering interactions with adaptor proteins.

## RESULTS

### Phosphorylation of KLC1, but not JIP1b, regulates the interaction between KLC1 and JIP1b

To investigate whether phosphorylation of KLC1 or JIP1b regulates the interaction between KLC1 and JIP1b, we first increased the phosphorylation level of both proteins by treating cells with okadaic acid (OA), a potent inhibitor of protein phosphatases 1 and 2A. COS7 cells expressing either HA-KLC1 or FLAG-JIP1b were cultured in the presence or absence of OA, and the respective cell lysates were combined to assess the association of KLC1 with JIP1b (Figure 1). In lysates of cells treated with OA, elevated phosphorylation of JIP1b was reflected by an obvious reduction in mobility in immunoblots (Figure 1A). No such decrease in mobility was apparent for HA-KLC1, but the elevated phosphorylation of this protein was confirmed in a Phos-tag–based mobility shift assay (Figure 1C).

When HA-KLC1 in lysates of cells treated with OA was combined with FLAG-JIP1b in lysates of cells treated with or without OA, the ability of KLC1 to bind JIP1b decreased significantly, as demonstrated by coimmunoprecipitation with anti-FLAG antibody. By contrast, binding of KLC1 to JIP1 was not diminished when FLAG-JIP1b in lysates of cells treated with or without OA was combined with HA-KLC1 in lysates of cells not treated with OA. In contrast, the association with HA-KLC1 with FLAG-JIP1b was strengthened in lysates from cells treated with OA (Figure 1, A and B). These results suggest that phosphorylation of KLC1 suppresses the interaction between KLC1 and JIP1b, whereas phosphorylation of JIP1b promotes it. Because phosphorylation of KLC1 had a major suppressive effect on the interaction with JIP1b, we further analyzed the effect of this modification.

To confirm that phosphorylation of KLC1 suppresses the interaction with JIP1b, and dephosphorylation of KLC1 restores the association, we performed in vitro pull-down assays with GST-JIP1b$^{351–707}$ fusion protein, which lacks the amino-terminal half of JIP1b but includes all domains and motifs required for the interaction with KLC1 (Chiba *et al.*, 2014a). FLAG-KLC1 protein purified from lysates of cells treated with OA bound less strongly to GST-JIP1b$^{351–707}$ than FLAG-KLC1 from lysates treated without OA (Figure 1D). However, when lysates of cells treated with OA were treated with λ phosphatase (PPase), the amount of FLAG-KLC1 bound to GST-JIP1b$^{351–707}$ was comparable to that in samples not treated with OA (Figure 1, D and E). These results clearly indicate that OA increases the phosphorylation level of KLC1 in cells and that phosphorylation of KLC1 suppresses the interaction with JIP1b.

The suppressive effect of OA on the binding of KLC1 to JIP1b was not complete. This is because the interaction between KLC1 and JIP1b requires multiple subdomains, involving a conventional interaction between the JIP1b C11 region and the KLC1 TPR region, as well as a novel interaction between the central region of JIP1b and the coiled-coil domain of KLC1 (Chiba *et al.*, 2014a). The partial inhibition of KLC1–JIP1b binding by KLC1 phosphorylation suggests that either, but not both, of these interactions is regulated by KLC1 phosphorylation. To explore this idea further, we sought to identify the phosphorylation site(s) of KLC1.

### Detection of phosphorylated amino acids in KLC1 in cells treated with OA

To determine which amino acids of KLC1 are phosphorylated, we performed multidimensional LC/MS-based analysis. First, we immunoprecipitated FLAG-KLC1 from lysates of cells treated with OA and resolved the isolated protein by SDS–PAGE. The KLC1 band was cut out and subjected to in-gel tryptic digestion. Because we could not exclude the possibility that phosphorylation occurs at

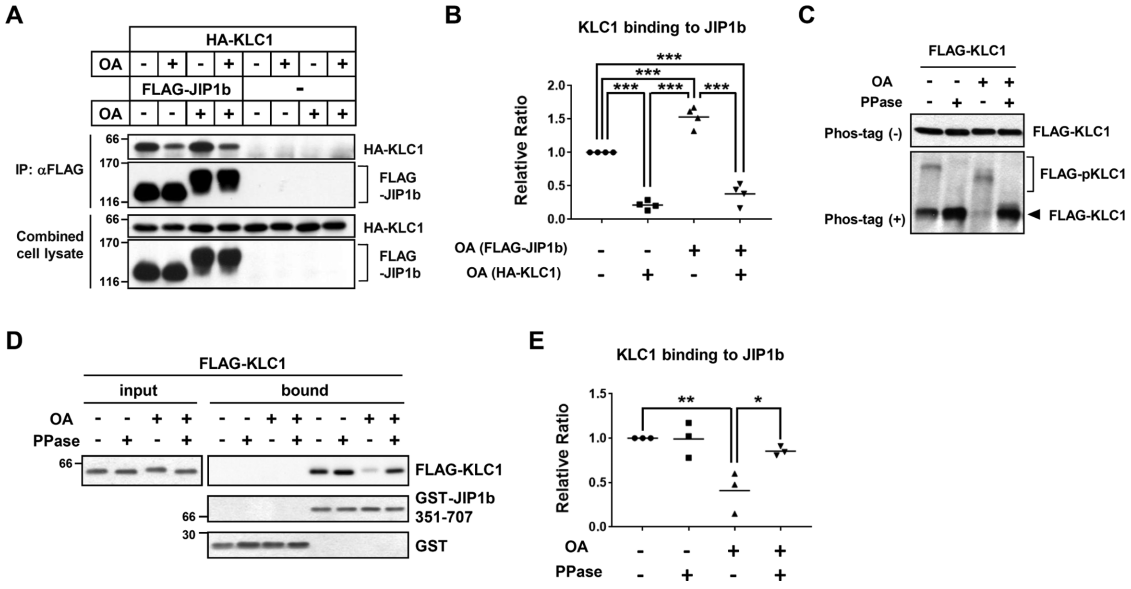


FIGURE 1: Phosphorylation of KLC1 regulates the interaction of KLC1 with JIP1b. (A) Association of KLC1 with JIP1b in cells treated with or without a protein phosphatase inhibitor. COS7 cells expressing HA-KLC1 or FLAG-JIP1b were cultured for 3 h in the presence (+) or absence (–) of 400 nM okadaic acid (OA). Cell lysate (200 μg of protein) containing HA-KLC1 was combined with the same amount of cell lysate containing FLAG-JIP1b, and the combined lysates were subjected to immunoprecipitation with anti-FLAG antibody. The combined cell lysates (10 μg) and immunoprecipitates (IP) were analyzed by immunoblotting with anti-FLAG and anti-HA antibodies. (B) Quantification of HA-KLC1 bound to FLAG-JIP1b in the various combinations shown in (A). Levels of HA-KLC1 recovered by immunoprecipitation with anti-FLAG antibody along with FLAG-JIP1b were quantified, and the binding of KLC1 to JIP1 is shown as a ratio. The binding ratio in a mixture of cell lysates containing FLAG-JIP1b and HA-KLC1 in the absence of OA treatment is defined as 1.0. Data are shown as means ± SD. Statistical significance was determined by Tukey's multiple comparison test ($n = 4$), and $p$ values are indicated (***, $p < 0.001$). (C) Phos-tag based mobility-shift assay of KLC1. COS7 cells expressing FLAG-KLC1 were treated with OA as described in A, and FLAG-KLC1 was recovered from cell lysates by immunoprecipitation with anti-FLAG antibody and treated with (+) or without (–) λ phosphatase (PPase). The immunoprecipitates were subjected to electrophoresis in the presence or absence of Phos-tag and analyzed by immunoblotting with anti-FLAG antibody. (D) Association of dephosphorylated KLC1 with JIP1b$^{351–707}$. COS7 cells expressing FLAG-KLC1 were cultured in the presence (+) or absence (–) of OA as described in A, and the cell lysates were further treated with (+) or without (–) λ protein phosphatase (PPase, 200 units) for 1 h. FLAG-KLC1 was recovered from the lysates by immunoprecipitation with anti-FLAG antibody, and 500 ng protein was examined for JIP1b binding by pulldown assay using glutathione beads plus either GST-JIP1b$^{351–707}$ or GST alone. Inputs (10 ng protein) and proteins bound to beads were detected by immunoblotting with anti-FLAG and anti-GST antibodies. (E) Quantification of HA-KLC1 bound to GST-JIP1b$^{351–707}$ in the combinations shown in D. The levels of KLC1 bound to JIP1b$^{351–707}$ are expressed as ratios. The ratio for cells not treated with OA in lysate not treated with PPase is defined as 1.0. Data are shown as means ± SD. Statistical significance was determined by Dunnett's multiple comparison test ($n = 3$), and $p$ values are indicated (*, $p < 0.05$; **, $p < 0.01$). (A, D) Numbers indicate protein size markers (in kilodaltons).

multiple sites, and because identification of the phosphorylation site(s) might be affected by heterogeneity within the pool, we performed a second round of separation: after extraction from the SDS gel, peptides were further fractionated, with or without phosphopeptide enrichment, by the immobilized metal affinity chromatography (IMAC) and/or $TiO_2$ methods. The peptides from each fraction were subjected to analysis and the results were compiled. This analysis identified 17 residues of KLC1 as candidate phosphorylation sites (Figure 2A). Nine of the 17 residues (Ser460, Ser462, Thr464, Thr466, Ser515, Ser521, Ser524, Tyr532, and Ser534) were located in the sixth TPR motif or the C-terminal region and were thus potentially involved in the interaction with JIP1b C11. For example, three (Ser460, Thr462, and Thr464) were phosphorylated in the tryptic fragment 458-V-D-S-P-T-V-T-T-T-L-K-468; representative MS spectra are shown in Figure 2B. This analysis indicated that multiple residues within the sixth TPR motif and the C-terminal region are subject to phosphorylation.

When conventional interaction between KLC1 and JIP1b is impaired, the association between KLC1 and JIP1b persists due to a novel interaction between the coiled-coil domain of KLC1 and the central region of JIP1b, as we reported previously (Chiba *et al.*, 2014a). Those results suggest that phosphorylation at one or more residue(s) of the nine candidates negatively regulates the conventional interaction between KLC1 and JIP1b, consistent with our observation that phosphorylation of KLC1 attenuates, but does not completely inhibit, the interaction with JIP1b (Figure 1).

### Identification of the phosphorylation sites of KLC1 that attenuate the association with JIP1b

LC-MS/MS analysis revealed several novel phosphorylatable residues in the sixth TPR region. To determine the residue(s) whose phosphorylation regulates the association with JIP1b, we next performed binding studies of proteins harboring amino acid substitutions at each of the candidate positions.

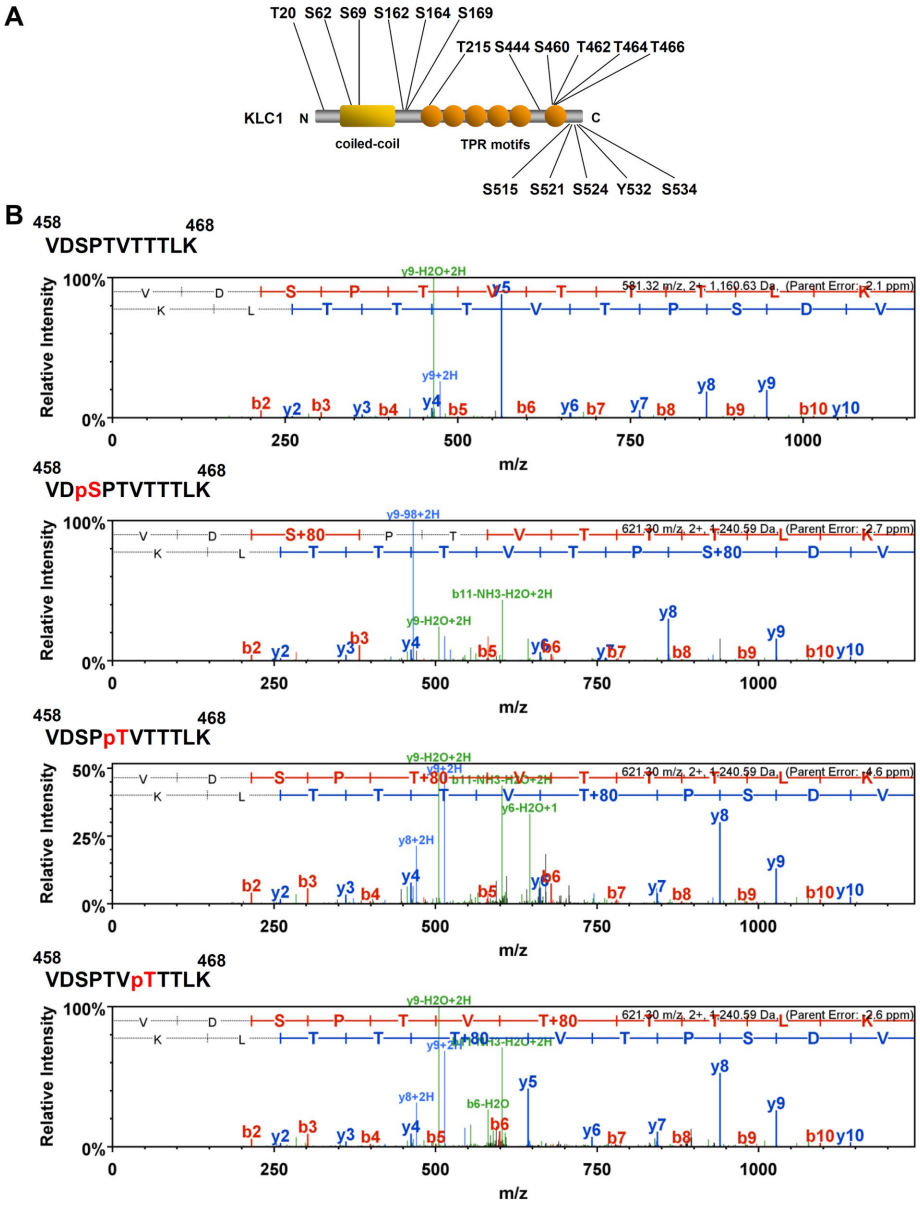


FIGURE 2: Identification of KLC1 phosphorylation sites by LC-MS analysis. (A) Phosphorylation sites of KLC1. Multidimensional sample preparation, including SDS–PAGE separation, phosphopeptide enrichment, and LC-MS/MS analysis, was performed for phosphorylated peptides from FLAG-KLC1 purified from OA-treated COS7 cells. A total of 17 phosphorylation sites were identified in the purified KLC1 samples. (B) Representative MS/MS spectra of a tryptic peptide, KLC1$^{458–468}$. Spectra with MS/MS fragmentation of peptide 458–468 are shown: $NH_2$-V-D-S-P-T-V-T-T-T-L-K-COOH (first row, nonphosphopeptide), $NH_2$-V-D-pS-P-T-V-T-T-T-L-K-COOH (second row, peptide phosphorylated at Ser460), $NH_2$-V-D-S-P-pT-V-T-T-T-L-K-COOH (third row, peptide phosphorylated at Thr462), and $NH_2$-V-D-S-P-T-V-pT-T-T-L-K-COOH (fourth row, peptide phosphorylated at Thr464).

HA-KLC1 variants harboring the indicated alanine or glutamic acid substitutions for residues Ser460, Thr462, Thr464, Thr465, and Thr466 in the sixth TPR region were expressed in Neuro 2a (N2a) cells along with FLAG-JIP1b, and the proteins were coimmunoprecipitated with anti-FLAG antibody. Immunoprecipitates (IP) and cell lysates (Lysate) were analyzed by immunoblotting with anti-FLAG and anti-HA antibodies (Figure 3). Taking into account the possibility of phosphorylation at multiple residues, we first examined KLC1 mutants harboring multiple Ala or Glu substitution at all five residues (Figure 3A). KLC1 mutants in which Ser460 was replaced with Ala or Glu were examined separately, because a previous study showed that phosphorylation at Ser460 does not modulate the KLC1–JIP1 interaction (Vagnoni *et al.*, 2011). Ala substitutions at all five residues did not alter KLC1 binding to JIP1b, nor did the S460A mutation alone (Figure 3B, left, Ala mutant). In contrast, Glu substitution of residues Thr462, Thr464, and Thr466 significantly weakened the KLC1–JIP1b association, whereas Glu substitution of Ser460 had no significant effect (Figure 3B, left, Glu mutant). These results suggest that phosphorylation of one or more of the three Thr residues regulates the interaction between JIP1b and KLC1. To identify the phosphorylation site responsible for binding, we examined KLC1 mutants in which Thr462, Thr464, and Thr466 were individually replaced by Glu (Figure 3B, right). Of the single-replacement mutants, only Thr466Glu (T466E) significantly decreased the interaction with JIP1b, as did substitution of all three residues (T462E/T464E/T466E) (Figure 3B, right), strongly suggesting that phosphorylation of KLC1 at Thr466 is primarily responsible for regulating the interaction with JIP1b. We noted that HA-KLC harboring T466E tended to be expressed in cells at lower levels than the other versions of the protein (Lysate in Figure 3B, right). FLAG-JIP1b expressed in the absence of the binding partner KLC1 also tended to be unstable (unpublished data). Both proteins in their unbound state may therefore be susceptible to proteolytic degradation in cells, in contrast to the bound form of KLC1 with JIP1b.

A recent study showed that Asn343 in the TPR domain of KLC1 is located within a binding pocket of the 11-amino acid C-terminal region of JIP1b (C11), which contains Tyr705 (Zhu *et al.*, 2012), a residue that is critical for the conventional interaction with KLC1 (Chiba *et al.*, 2014a). The N343S mutation decreases the binding affinity to JIP1b, as determined by thermodynamic parameters (Zhu *et al.*, 2012). Therefore, we compared the importance of the Thr466 residue of KLC1 for the interaction with JIP1b with that for the JIP1b-binding ability of KLC1 with the Asn343Ser mutation (N343S). As shown in Figure 3C, KLC1 N343S exhibited a very weak association with JIP1b, as expected. Interestingly, KLC1 T466E also exhibited a weaker association with JIP1b than KLC1 wild type (WT). In contrast, the T466A mutation did not alter the strength of binding to JIP1b.

These results demonstrate that the association between KLC1 and JIP1b is more complex than suggested by a previous model (Verhey *et al.*, 2001), in which binding is mediated by an interaction between JIP1b C11 and the tetratricopeptide repeat (TPR) of KLC1. This conventional interaction is required for the EFV of anterograde transport of APP cargo by kinesin-1 in axons (Chiba *et al.*, 2014a). If

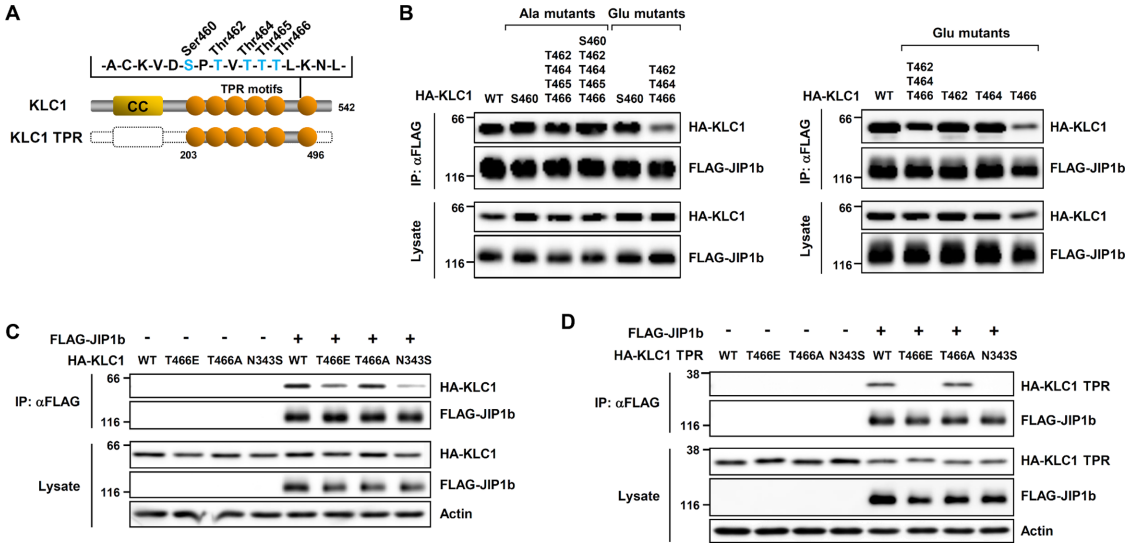


FIGURE 3: Effects of phosphorylatable amino acid residues in the sixth TPR of KLC1 on the interaction with JIP1b. (A) Structure of mouse KLC1 (top) and KLC1 TPR (bottom) proteins used in this study, and the amino acid sequence of the sixth TPR motif, including five phosphorylatable amino acids (blue). The "CC" in the rectangle indicates the coiled-coil/heptad repeats region, and the ovals indicate the six TPR motifs. KLC1 TPR is a truncated form of KLC1 that lacks the 202 amino-terminal and 46 carboxyl-terminal amino acids. (B) Coimmunoprecipitation of KLC1 and JIP1b. HA-KLC1 (WT) and various HA-KLC1 proteins in which Ala or Glu replaced phosphorylatable Ser (S) or Thr (T) residues were expressed in N2a cells along with FLAG-JIP1b. Cell lysates were subjected to immunoprecipitation with anti-FLAG antibody, and the lysates (10 µg protein) and immunoprecipitates (IP) were analyzed by immunoblotting with anti-HA and anti-FLAG antibodies. Representative blots are shown. (C) Coimmunoprecipitation of KLC1 and JIP1b. HA-KLC1 (WT) and HA-KLC1 protein harboring the Thr466Glu, Thr466Ala, or Asn343Ser substitution were expressed in N2a cells with (+) or without (–) FLAG-JIP1b, and KLC1 binding to JIP1b was analyzed as described in B. A representative blot is shown along with a blot for actin (as a loading control). (D) Coimmunoprecipitation of KLC1 TPR and JIP1b. HA-KLC1 TPR (WT) and HA-KLC1 TPR proteins harboring the Thr466Glu, Thr466Ala, or Asn343Ser substitution were expressed in N2a cells with (+) or without (–) FLAG-JIP1b, and KLC1 TPR-binding to JIP1b was analyzed as described above. A representative blot is shown along with a blot for actin. (B–D) Numbers indicate protein size markers (in kilodaltons).

this conventional interaction and the EFV transport of APP cargo are impaired, the association between KLC1 and JIP1b is preserved only by novel interactions between the N-terminal coiled-coil region of KLC1 and two regions of JIP1b, JIP1b$^{370–402}$ and JIP1b$^{465–483}$ (Chiba *et al.*, 2014a). Thus, KLC1 harboring T466E or N343S, which both affect the conventional interaction with JIP1b, can maintain a weak association with JIP1b (Figure 3C). Accordingly, we investigated the JIP1b interactions of the KLC1 TPR region, which lacks the N-terminal coiled-coil region (KLC1$^{1–202}$) and the C-terminal tail region (KLC1$^{497–542}$) (Figure 3A), harboring T466E, T466A, or N343S (Figure 3D). Again, KLC1 TPR harboring T466A retained the association with JIP1b, as did the WT KLC1 TPR region. In contrast, KLC1 TPR harboring T466E or N343S completely lost the ability to interact with JIP1b (Figure 3D). This result clearly shows that Thr466 of KLC1 is critically involved in regulation of the interaction with JIP1b C11 and that a negative charge at position 466 (due to either amino acid substitution or phosphorylation) abolishes the conventional association between the JIP1b C11 and the KLC1 TPR region.

## Phosphorylation of KLC1 at Thr466

To demonstrate that KLC1 is phosphorylated at Thr466 in neuronal tissues in vivo and to reveal the phosphorylation state of KLC1 in association with JIP1b, we developed a phosphorylation state–specific antibody against Thr466 of KLC1 (anti-pKLC1). Affinity-purified antibody was tested for phosphorylation state specificity by an enzyme-linked immunosorbent assay (ELISA). In these experiments, the indicated amounts of antigen peptide KLC1$^{462–470}$ phosphorylated at Thr466 were reacted with purified antibody along with nonphosphorylated KLC1$^{462–470}$ peptide and an unrelated amyloid precursor-like protein 2 peptide, APLP2$^{732–740}$, phosphorylated at Thr736 (Suzuki *et al.*, 1997; Figure 4A). Anti-pKLC1 reacted exclusively with the KLC1$^{462–470}$ peptide phosphorylated at Thr466, not with nonphosphorylated KLC1$^{462–470}$ or APLP2$^{732–740}$ phosphorylated at Thr736, indicating that anti-pKLC1 specifically recognized KLC1 phosphorylated at Thr466.

Next, we investigated whether the anti-pKLC1 antibody recognized the intact KLC1 protein. Because we anticipated that the level of KLC1 phosphorylated at Thr466 would not be constitutively high, we treated N2a cells expressing FLAG-KLC1 with OA to increase the phosphorylation level. Cell lysates were subject to immunoprecipitation with anti-FLAG antibody, and the immunoprecipitates were analyzed by immunoblotting with anti-pKLC1 and anti-FLAG antibodies. Anti-pKLC1 antibody clearly detected a band at the predicted molecular weight of KLC1 (~60 kDa; Figure 4B), and the signal disappeared when the immunoprecipitate was treated with λ protein phosphatase (PPase). These data indicate that KLC1 is phosphorylated at Thr466 in cells, at least when the activity of intracellular serine/threonine protein phosphatases is suppressed by OA.

We next confirmed that pKLC1 antibody recognizes KLC1 phosphorylated at Thr466, but not KLC1 phosphorylated at other residues. For this purpose, N2a cells expressing WT FLAG-KLC1 and FLAG-KLC1 harboring T466A or T466E were treated with or without

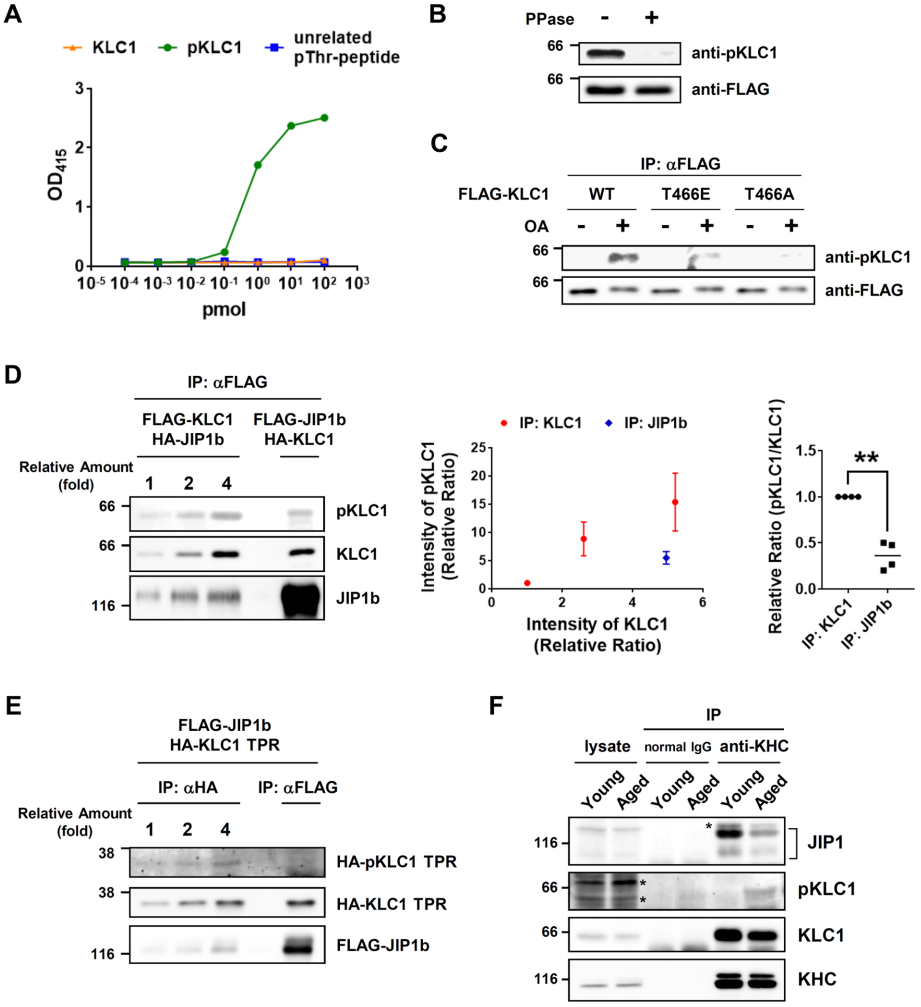


FIGURE 4: KLC1 is phosphorylated at Thr466 in the brain, and the phosphorylation level within the kinesin-1 complex increases with aging. (A) Specificity of the anti-pKLC1 [pThr466] antibody. Phosphorylation state specificity of anti-pKLC1 [pThr466] antibody (anti-pKLC1 antibody; 0.05 μg IgG) was examined by ELISA using the indicated amounts of KLC1$^{462–470}$ peptides with (circle) or without (triangle) phosphate at Thr466, and an unrelated phosphopeptide, APLP2$^{732–740}$, phosphorylated at Thr736 (square). Immunoreactive bands were detected with horseradish peroxidase (HRP)-conjugated anti-rabbit antibody, and tetramethylbenzidine was used to colorimetrically detect antigen–antibody complex by measuring $OD_{415}$. (B) Detection of KLC1 phosphorylated at Thr466. N2a cells expressing FLAG-KLC1 were treated with OA (400 nM) for 3 h and lysed for immunoprecipitation with anti-FLAG antibody. The immunoprecipitates were treated with (+) or without (–) λ protein phosphatase (PPase) and analyzed by immunoblotting with anti-pKLC1 (top) and anti-FLAG (bottom) antibodies. (C) Reactivity of anti-pKLC1 antibody toward KLC1 harboring the Thr466Glu or Thr466Ala substitution. N2a cells expressing FLAG-KLC1 (WT) or FLAG-KLC1 harboring T466E or T466A were treated with (+) or without (–) OA as described in B. FLAG-KLC1 was recovered by immunoprecipitation with anti-FLAG antibody and analyzed by immunoblotting with anti-pKLC1 (top) and anti-FLAG (bottom) antibodies. (D) Reduced phosphorylation of KLC1 in complex with JIP1b. To determine the phosphorylation state of KLC1 at Thr466 within a complex associated with JIP1b, FLAG-KLC1 and HA-JIP1b or FLAG-JIP1b and HA-KLC1 were coexpressed in N2a cells and treated with OA (400 nM) for 3 h, cell lysates were subjected to immunoprecipitation with anti-FLAG antibody, and the coimmunoprecipitated HA-JIP1b and FLAG-KLC1 or HA-KLC1 and FLAG-JIP1b were analyzed by immunoblotting with anti-pKLC1, anti-KLC1, and anti-JIP1 antibodies (left panel). A linear relationship between band intensities of KLC1 phosphorylated at Thr466 and those of KLC1 was observed in a dose-dependent manner of immnunoprecipitates (×1-, ×2- and ×4-fold) when FLAG-KLC1 was expressed in cells (circle), and the level of KLC1 phosphorylated at Thr466 was shown when HA-KLC1 was expressed in cells (diamond) (middle panel). Phosphorylation level, as a proportion of overall amount of HA-KLC1 co-immunoprecipitated with FLAG-JIP1b, was estimated and compared with the level of FLAG-KLC1 recovered by immunoprecipitation with anti-FLAG antibody; the result is expressed as a ratio (pKLC1/ KLC1) (right panel). Statistical analysis used Student's *t* test ($n = 4$; **, $p < 0.01$). (E) Coimmunoprecipitation of KLC1 TPR with JIP1b. HA-KLC1 TPR (see Figure 3A) was expressed in N2a cells with FLAG-JIP1b, lysed, and subjected to immunoprecipitation with anti-HA or anti-FLAG antibody. Precipitated KLC1 TPR, pKLC1 TPR, and JIP1b were detected by immunoblotting with the indicated antibodies. (F) Elevated phosphorylation of KLC1 of kinesin-1 in aged brain. Brain lysates were prepared from young (2-mo-old) and aged (22-mo-old) mice and subjected to immunoprecipitation with anti-KHC antibody and identical amounts of normal IgG (5 μg). The immunoprecipitates (IP) and lysates (20 μg protein) were analyzed by immunoblotting with anti-KHC, anti-KLC1, anti-pKLC1, and anti-JIP1 antibodies. Asterisk (*) indicates nonspecific products. Representative blots are shown. (B–F) Numbers indicate protein size markers (in kilodaltons).

OA and lysed. FLAG-KLC1 was recovered from the cell lysate by immunoprecipitation with anti-FLAG antibody and analyzed by immunoblotting with anti-pKLC1 and anti-FLAG antibodies (Figure 4C). WT KLC1 yielded a strong signal with anti-pKLC1 antibody when cells were treated with OA, whereas the signal for T466E or T466A was reduced to background levels irrespective of OA treatment. These data indicate that the anti-pKLC1 antibody predominantly recognizes KLC1 phosphorylated at Thr466.

The results of the cellular studies suggested that the constitutive phosphorylation level of KLC1 may be low in vivo. We estimated the levels of KLC1 phosphorylation at Thr466 with a combination of immunoblot and dot blot analysis using anti-KLC1 and anti-pKLC1 antibodies (Supplemental Figure S1). Various amounts of KLC1$^{154–172}$ or KLC1$^{462–470}$ (with phosphate at Thr466) were spotted on nitrocellulose membrane and probed with anti-KLC1 (UT109) or anti-pKLC1 antibodies, followed by HRP-conjugated second antibody, and the luminescence was quantitated to draw standard curves (Supplemental Figure S1A). FLAG-KLC1 was recovered from N2a cells with or without OA treatment by immunoprecipitation with anti-FLAG antibody, analyzed by immunoblotting with anti-KLC1 and anti-pKLC1 antibodies, followed by the HRP-conjugated second antibody. The luminescence was quantified, and protein and phosphorylation levels of FLAG-KLC1 were calculated to estimate the levels of KLC1 phosphorylation at Thr466 (Supplemental Figure S1B, right graph). The phosphorylation of KLC1 at Thr466 was very low in the absence of OA and was increased ~25-fold in the presence of OA.

We speculated that, in comparison with free KLC in cytoplasm, KLC in the kinesin-1 heterotetramer associating with JIP1b is likely more dephosphorylated; this idea was supported by the observation that the phosphomimetic substitution of Glu for Thr466 weakened the interaction between KLC1 and JIP1b (Figure 3). To explore this possibility further, we compared the phosphorylation level of KLC1 bound to JIP1b with that of total KLC1, including free KLC1 molecules. For this purpose, N2a cells transiently coexpressing FLAG-KLC1 and HA-JIP1b or FLAG-JIP1b and HA-KLC1 were cultured in the presence of OA. The cell lysates were subjected to immunoprecipitation with anti-FLAG antibody, and the immunoprecipitated KLC1, pKLC1, and JIP1b were detected by immunoblotting with the appropriate antibodies (Figure 4D, left). Band intensities of KLC1 and pKLC1 were calculated as the ratio relative to the amount of the furthest left lane (given a value of 1.0), and the levels of KLC1 were normalized to the levels of pKLC1 to show the relationship between KLC1 and pKLC1 levels (Figure 4D, middle). The phosphorylation level of FLAG-KLC1 increased linearly with the amount of FLAG-KLC1 even when HA-JIP1 was coexpressed (circles in the middle panel). When HA-KLC1 was coimmunoprecipitated with FLAG-JIP1b using anti-FLAG antibody, the relative ratio of pKLC1 to KLC1 was significantly lower (Figure 4D, right) compared with the relative ratio observed following immunoprecipitation of FLAG-KLC1.

The result suggests that unphosphorylated KLC1 associates preferentially with JIP1b, although KLC1 can interact with JIP1b via the novel interaction between the KLC1 coiled-coil region and the JIP1b$^{370–402}$ and JIP1b$^{465–483}$ regions, irrespective of KLC1 phosphorylation at Thr466 (Figure 3, C and D). Hence, we next performed experiments using FLAG-KLC1 TPR and HA-KLC1 TPR, which lack the coiled-coil region involved in the novel interaction (Figure 4E). The level of KLC1 TPR phosphorylated at Thr466 in association with JIP1b was negligible (see the rightmost lane of Figure 4E) in comparison with the level of total KLC1 TPR, including free KLC1 TPR, isolated with anti-HA antibody. In other words, phosphorylation of KLC1 at Thr466 suppressed the conventional interaction with JIP1b.

Using the anti-pKLC1 antibody, we investigated whether KLC1 is phosphorylated at Thr466 in brain tissues in vivo. To this end, we isolated kinesin-1 from cerebrum lysates of young (2 mo) and aged (22 mo) mice by immunoprecipitation with anti-KHC antibody; an identical amount of nonimmune normal immunoglobulin G (IgG) was used as a negative control. Immunoprecipitates and lysates were analyzed by immunoblotting with anti-KHC, anti-KLC1, anti-pKLC1, and anti-JIP1 antibodies. In samples from young mice, anti-KHC antibody recovered both KLC1 and JIP1, but KLC1 phosphorylated at Thr466 was undetectable. In contrast, in samples from aged mice, the recovery of JIP1 was significantly reduced but KLC1 phosphorylated at Thr466 was present (Figure 4F). Endogenous brain JIP1 showed two protein bands by immunoblotting. Both signals were JIP1 splicing variants, because the two proteins were not detected in brain lysate of JIP1-KO mice (unpublished data). This result indicates that KLC1 is phosphorylated at Thr466 in brain in vivo and that the phosphorylation level of this protein is undetectable or very low in the kinesin-1 complex associated with JIP1 in young mice. Moreover, in aged mice, the phosphorylation level was elevated, and the association of JIP1 with kinesin-1 was attenuated. The result suggests that the increased phosphorylation of KLC1 of kinesin-1 heterotetramer suppresses the conventional interaction of JIP1 with kinesin-1 in aged mice.

### APP anterograde transport by kinesin-1 complex including phosphomimetic KLC1

JIP1 is an essential factor for the EFV of APP axonal transport by kinesin-1, and the velocity of APP anterograde transport is reduced in JIP1-deficient neurons (Chiba *et al.*, 2014a). The velocity of APP fast transport in the absence of JIP1 is similar to that of kinesin-1 moving on microtubules in vitro (Kawaguchi and Ishiwata, 2000) or that of the fast transport of Alcα cargo connected directly to KLC1 (Araki *et al.*, 2007; Kawano *et al.*, 2012). Therefore, JIP1b plays an important role in the connection of APP to kinesin-1, which contributes to the EFV and the EHF of APP anterograde transport.

To investigate the roles of Thr466 of KLC1 in APP anterograde transport by kinesin-1, we used differentiating CAD cells (mouse catecholaminergic neuroblastoma). These cells can elongate neurites, permitting examination of anterograde cargo transport by kinesin-1 (Araki *et al.*, 2007). First, we confirmed that the enhanced fast transport of APP cargoes mediated by JIP1b occurred in the differentiating CAD cells, as observed in primary cultured neurons (Chiba *et al.*, 2014a). Cells expressing APP-EGFP, with or without small interfering RNA (siRNA) against JIP1 (siJIP1) vector, were analyzed for anterograde transport of APP cargo in neurites (Figure 5, A and B; see Supplemental Movies 1 and 2); the knockdown efficiency of siJIP1 is shown in Supplemental Figure S2. The expression level of JIP1 decreased by 38% in cells treated with siJIP1 from that in cells without siJIP1. Approximately 60% of the APP cargoes were transported in an anterograde manner, whereas 10% were transported retrogradely and 30% were stationary (Figure 5A). When JIP1 expression was knocked down, the velocity of anterograde transport of APP decreased (1.57 ± 0.56 μm/s, Figure 5B; see also Supplemental Movie 2) relative to the control (2.03 ± 0.77 μm/s, Figure 5A; see also Supplemental Movie 1), and the difference in velocity was statistically significant ($p < 0.0001$). The knockdown of JIP1 expression also increased retrograde transport of APP to 18%, and the increase was significant ($p = 0.04$; compare bar graphs in Figure 5, A and B). These results indicate that JIP1 promotes the EFV of APP anterograde transport along with preserving EHF of APP anterograde transport in differentiating CAD cells, as it does in primary cultured neurons. The reduced velocity of APP cargo transport was restored by expression of wild-type JIP1b$^{R}$, an siRNA-resistant form (2.08 ± 0.82 μm/s, Figure 5C; see also Supplemental Movie 3) ($p < 0.0001$), but not by expression of a mutant JIP1b$^{R}$ Y705A (1.60 ± 0.50 μm/s, Figure 5D; see also Supplemental Movie 4), which inhibits the conventional interaction between the JIP1b C11 and KLC1 TPR regions, resulting in reduced velocity (Chiba *et al.*, 2014a). Expression of WT HA-JIP1b$^{R}$ or HA-JIP1b$^{R}$ Y705A was not knocked down by expression of JIP1b siRNA (Supplemental Figure S2).

Expression of WT JIP1b$^{R}$ tends to decrease the frequency of APP retrograde transport by 12%, although this decrease was not significant ($p = 0.45$; compare Figure 5C with Figure 5B). Expression of a mutant JIP1b$^{R}$ Y705A showed a trend of decreased frequency of APP retrograde transport by 11%, as did expression of wild-type JIP1b$^{R}$ (compare Figure 5D with Figure 5C). This small effect (though significant) of the knockdown, yet lack of significant rescue, may be a reflection of the lower efficiency of knockdown in CAD cells as compared with knockout in neurons (see Chiba *et al.*, 2014a). These observations largely support our previous report that the conventional interaction between the JIP1b C11 and KLC1 TPR regions regulates EFV of APP anterograde transport by kinesins-1 (Chiba *et al.*, 2014a). Taken together, these findings confirmed that at least the velocity of anterograde transport of APP is increased by JIP1b in neurites of differentiating CAD cells, and that the interaction between the JIP1b C11 region, including Tyr705, and the KLC1 TPR region is essential for this increase in velocity, as previously shown in primary cultured neurons (Chiba *et al.*, 2014a).

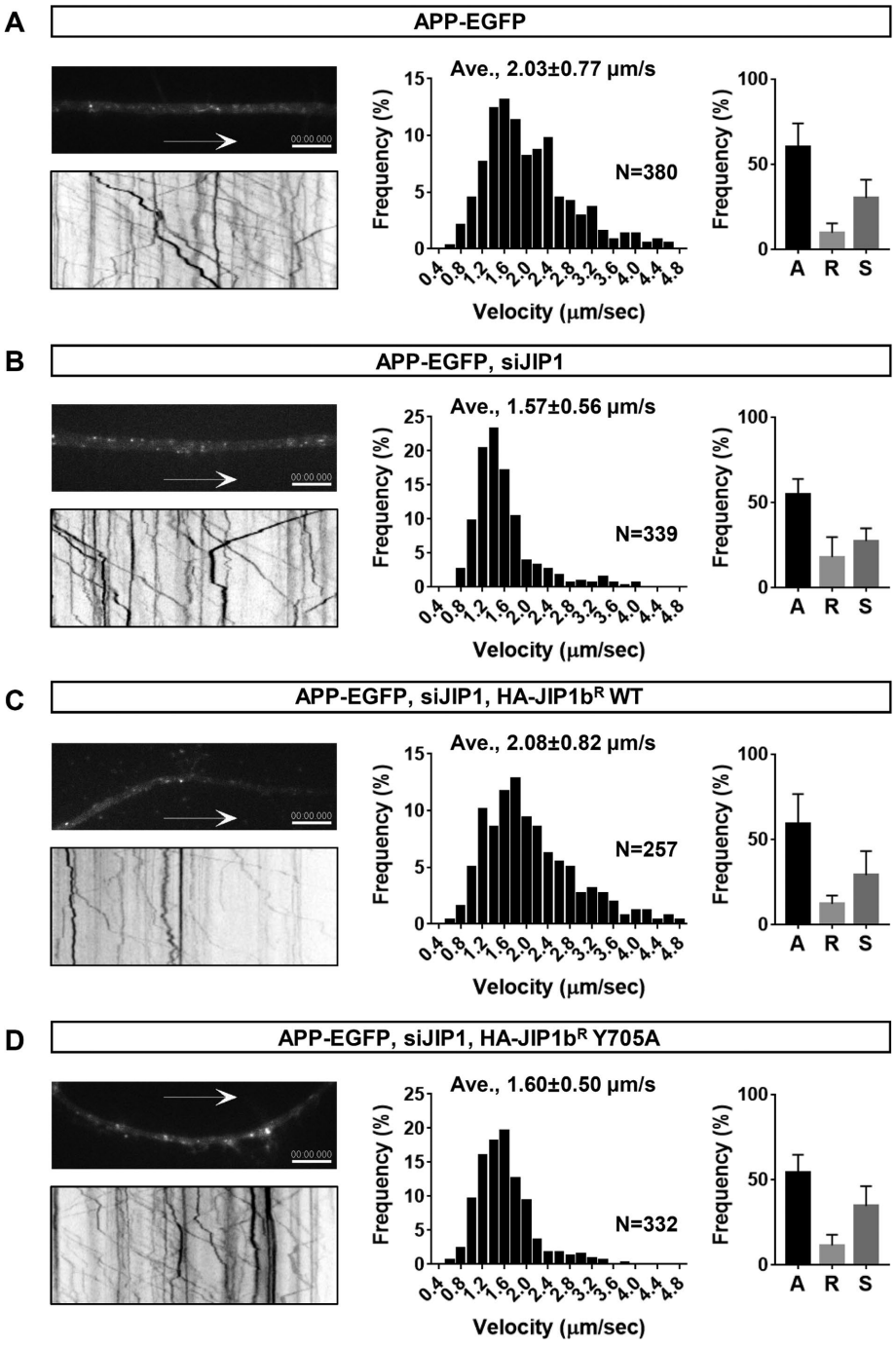


FIGURE 5: JIP1-dependent enhanced anterograde transport of APP vesicles in differentiating CAD cells. (A, B) APP-EGFP transport in neurites of differentiating CAD cells. APP-EGFP was expressed in CAD cells along with pSuper vector alone (A; see Supplemental Movie 1) or pSuper encoding siJIP1 (B; see Supplemental Movie 2). (C, D) APP-EGFP transport in neurites of differentiating CAD cells expressing siRNA-resistant HA-JIP1b$^R$ WT (C; see Supplemental Movie 3) or HA-JIP1b$^R$ Y705A (D; see Supplemental Movie 4) in the presence of siJIP1. (A–D) Transport of APP cargoes is depicted by movies (top left; see also Supplemental Movies 1–4), and the kymographs are shown to depict all vesicle movement (bottom left). The cumulative frequencies of velocities of anterograde transport of APP cargo are shown (middle panel; data are normalized as percentages). The proportions of anterograde (A), retrograde (R), and stationary (S) vesicles are indicated (right panel). Scale bar, 5 μm. Statistical analyses of cargo velocity distributions were performed using the Kruskal–Wallis test followed by Dunn's multiple comparison test, and the average velocity is shown along with the SD (±SD). Statistical significance: A vs .B, $p < 0.0001$; B vs. C, $p < 0.0001$; A vs. C, not significant. Direction of moving vesicles was analyzed by the $\chi^2$ test, followed by residual analysis.

We next sought to determine the function of residue Thr466 of KLC1 in APP cargo transport by kinesin-1 in differentiating CAD cells. For this purpose, we expressed APP-EGFP in differentiating CAD cells expressing siRNA-resistant FLAG-tagged WT KLC1 (FLAG-KLC1$^R$ WT) or mutant KLC1 harboring Thr466Glu or Thr466Ala (FLAG-KLC1$^R$ T466E or T466A) in the presence of siKLC1 and siKLC2 to deplete endogenous KLCs. We confirmed that endogenous KLC1 and KLC2 were knocked down by the siRNA in CAD cells, whereas expression of siRNA-resistant FLAG-KLC1$^R$ proteins persisted (Supplemental Figure S3). Upon depletion of KLCs (KLC1 plus KLC2) in cells, almost all APP cargoes stalled (i.e., became stationary) in the neurites with fewer retrograde transporting vesicles (Figure 6A; see also Supplemental Movie 5). This result supports the previous conclusion that APP is transported anterogradely by kinesin-1 in neurites (Araki *et al.*, 2007).

Expression of WT FLAG-KLC1$^R$ rescued the EFV transport (2.39 ± 0.82 μm/s) in cells depleted of endogenous KLCs (Figure 6B; see Supplemental Movie 6), indicating that moving APP cargoes were largely transported by kinesin-1, including KLC1$^R$ WT. APP cargoes were transported anterogradely at a velocity of 2.07 ± 0.85 μm/s in cells expressing the phosphomimetic mutant FLAG-KLC1$^R$ T466E (Figure 6C; see Supplemental Movie 7), significantly slower than in cells expressing FLAG-KLC1$^R$ WT (Figure 6B, Supplemental Movie 6; $p < 0.0001$). Average velocity (2.45 ± 0.83 μm/s) of anterograde transport of APP cargo in cells expressing FLAG-KLC1$^R$ T466A was similar to that in cells expressing FLAG-KLC1$^R$ WT (compare Figure 5D with Figure 5B; compare Supplemental Movie 8 with Supplemental Movie 6). The proportions of anterograde, retrograde, and stationary cargo did not differ significantly among cells expressing FLAG-KLC1$^R$ WT, FLAG-KLC1$^R$ T466E, and FLAG-KLC1$^R$ T466A, consistent with a previous report that conventional interaction between the JIP1b C11 and KLC1 TPR regions is required for the EFV of APP cargoes by kinesin-1, but not for the EHF of anterograde transport of APP cargoes (Chiba *et al.*, 2014a). Furthermore, it is reasonable that the conventional interaction between the JIP1b C11 and KLC TPR regions would be suppressed by replacement of Thr466 with Glu, creating a negative charge analogous to phosphorylation of KLC1 at Thr466, but not by replacement with Ala.

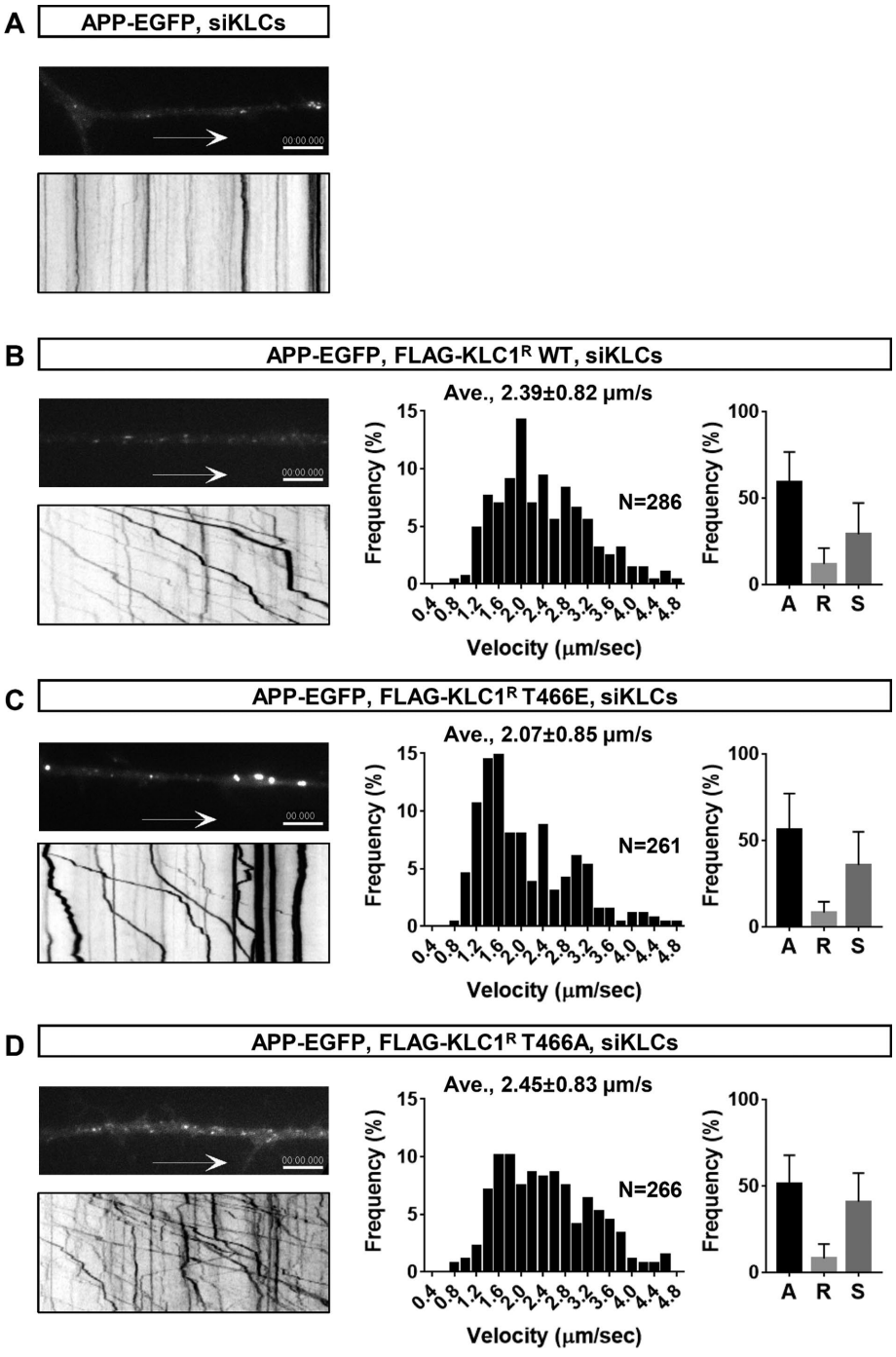


FIGURE 6: Phosphomimetic KLC1 T466E decreases the velocity of APP anterograde transport. (A) APP-EGFP transport in neurites of differentiating CAD cells in which KLC expression was knocked down. APP-EGFP was expressed in differentiating CAD cells in the presence of siKLC1 and siKLC2 (siKLCs; Supplemental Movie 5). (B–D) APP-EGFP transport in neurites of differentiating CAD cells in which endogenous KLC was knocked down in the presence of FLAG-KLC1WT or FLAG-KLC1 harboring T466E or T466A. siRNA-resistant FLAG-KLC1 (B, FLAG-KLC1$^{R}$WT; Supplemental Movie 6), FLAG-KLC1 harboring T466E (C, FLAG-KLC1$^{R}$T466E; Supplemental Movie 7), and FLAG-KLC1 harboring T466A (D, FLAG-KLC1$^{R}$T466A; Supplemental Movie 8) were exogenously expressed in cells. (A–D) Transport of APP cargoes is depicted in movies (top left; see Supplemental Movies 5–8), and their kymographs are shown to depict all vesicle movement (bottom left). (B–D) The cumulative frequencies of velocities of anterograde transport of APP cargo are shown (middle panel; data are normalized as percentages, and average velocities are shown with the SD [±SD]). Scale bar, 5 μm. Statistical analyses of cargo velocity distributions were performed as described in Figure 5. Statistical significance: B vs. C, $p < 0.0001$; C vs. D, $p < 0.0001$; B vs. D, not significant. The proportions of anterograde (A), retrograde (R), and stationary (S) vesicles are indicated (right panel).

To examine the KLC1 mutants in the kinesin-1 complex, we expressed WT HA-KLC1 or HA-KLC1 harboring T466E or T466A in N2a cells along with HA-JIP1b and KIF5C (KHC)-FLAG and then subjected cell lysates to immunoprecipitation with anti-FLAG antibody. The immunoprecipitates were analyzed by immunoblotting with anti-HA and anti-FLAG antibodies (Figure 7A). Similar levels of HA-KLC1 were recovered with KIF5C (KHC)-FLAG, indicating that the immunoprecipitation recovered kinesin-1. However, the recovery of JIP1b was significantly reduced in cells expressing KLC1 T466E in comparison with cells expressing KLC1 WT or KLC1 T466A (Figure 7B). These data indicate that KLC1 T466E forms a kinesin-1 heterotetramer with KHC/KIF5C, but that its association with JIP1b is weakened by the absence of conventional interaction between KLC1 and JIP1b. The decrease in velocity of APP cargo transport by kinesin-1 in cells expressing KLC1 T466E (Figure 6C) is likely due to the impairment of the conventional interaction, which is essential for the EFV of APP cargo transport.

## DISCUSSION

JIPs were first reported as cytoplasmic scaffold proteins of the c-Jun amino-terminal kinase (JNK) family (Dickens *et al.*, 1997) and subsequently as adaptor proteins that recruit motor proteins to membrane-bound cargoes (Meyer *et al.*, 1999; Stockinger *et al.*, 2000; Matsuda *et al.*, 2001; Verhey *et al.*, 2001; Taru *et al.*, 2002). In addition, several studies reported that JIP1 activates auto-inhibited kinesin-1 (Blasius *et al.*, 2007; Fu and Holzbaur, 2013) and plays an important role in efficient anterograde transport of APP cargo, including the EFV and the EHF of anterograde cargo transport by kinesin-1 (Chiba *et al.*, 2014a). To accomplish the efficient anterograde transport of APP cargo, the interactions between JIP1 and KLC are essential: the conventional interaction between KLC1 TPR motifs and the JIP1b C11 region is required for the EFV of APP anterograde axonal transport, whereas the novel interaction between the JIP1b central region and KLC1 coiled-coil domain is required for the EHF of anterograde transport of APP (Chiba *et al.*, 2014a) (schematically shown in Figure 8). However, the detailed regulation of the complex interactions between APP and JIP1 remains unclear.

Several studies have reported that protein phosphorylation is involved in regulating the interaction between cargoes and KIFs, including kinesin-1. Phosphorylation of KLC2 facilitates release of membrane cargoes from molecular motors at nerve

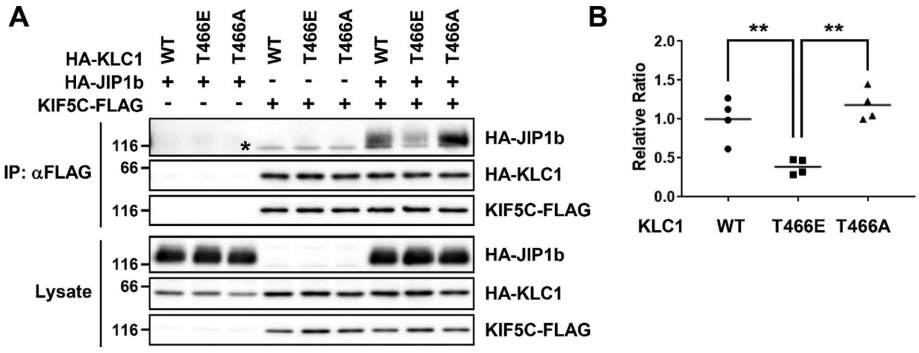


FIGURE 7: Phosphomimetic KLC1 in the kinesin-1 complex attenuates the interaction with JIP1b. (A) Coimmunoprecipitation of KLC1 in kinesin-1 and JIP1b. HA-KLC1 (WT) and HA-KLC1 harboring T466E or T466A was expressed in N2a cells along with HA-JIP1b in the presence or absence of KIF5C-FLAG. The cells were lysed and subjected to immunoprecipitation with anti-FLAG antibody, and the immunoprecipitates and lysates were analyzed by immunoblotting with anti-HA and anti-FLAG antibodies. A representative blot is shown. Numbers indicate protein size markers (in kilodaltons). (B) Quantification of HA-JIP1b bound to KLC1 (WT), KLC1 T466E, or KLC1 T466A within the kinesin-1. The levels of HA-JIP1b bound to kinesin-1 are expressed as ratios. The ratio in kinesin-1 included in KLC1 WT is defined as 1.0. Data are shown as means ± SD. Statistical significance was determined by Tukey's multiple comparison test ($n = 4$; **, $p < 0.01$).

terminals (Morfini *et al.*, 2002). When KLC1 is phosphorylated at Ser460, Alcα/calsyntenin1 cargo can dissociate from kinesin-1 (Vagnoni *et al.*, 2011), whereas multiple-site phosphorylation of Alcα is essential for the association with kinesin-1 (Sobu *et al.*, 2017). Phosphorylation of KIF17 by calcium/calmodulin-dependent protein kinase II releases Mint1/X11 protein from KIF17, which may contribute to spine formation on neuronal dendrites (Guillaud *et al.*, 2008).

The key observations of this study are as follows: 1) KLC1 phosphorylation plays a major role in regulating the association between KLC1 and JIP1b; 2) KLC1 phosphorylated at Thr466 suppresses the conventional interaction with the JIP1b C11 region, but does not influence the novel interaction between the central region of JIP1b and the coiled-coil domain of KLC1; 3) the level of KLC1 phosphorylated at Thr466 is elevated in aged brain, concomitant with attenuation of the association of JIP1b with kinesin-1; and 4) the EFV of APP cargo transport is impaired and the association with JIP1b is attenuated in neuronal cells expressing KLC1, in which Thr466 is replaced with Glu, a phosphomimetic form. Taken together, our findings indicate that phosphorylation of Thr466 suppresses the conventional interaction between the KLC1 TPR motif and JIP1b C11 (Figure 8), which is essential for the EFV of APP cargo transport (Chiba *et al.*, 2014a). Even if this conventional interaction is impaired, the APP cargo can still be transported by kinesin-1 via the novel interaction of JIP1b$^{370–402}$ and JIP1b$^{465–483}$ with the KLC1 coiled-coil domain, although the EFV of APP cargo transport is abolished (Chiba *et al.*, 2014a).

Using a phosphospecific antibody, we demonstrated that endogenous KLC1 is phosphorylated at Thr466 in mouse brain. Notably, another group previously reported the phosphorylation of KLC1 at Thr466 in mouse pancreas (Huttlin *et al.*, 2010), suggesting that this phosphorylation event may regulate the association of other cargoes with kinesin-1 motors in nonneuronal cells.

Ser460 of KLC1 is phosphorylated by extracellular signal-regulated kinase (ERK) in vitro, and this phosphorylation may regulate the binding of KLC1 to Alcα/calsyntenin-1 (Vagnoni *et al.*, 2011). In our LC-MS/MS analyses, we identified Ser460 as a phosphorylated residue in a trypsin-digested phosphopeptide. Because we could not clearly detect double phosphorylation at Ser460 and Thr466 residues within this phosphopeptide, we postulate that the two sites are phosphorylated in a mutually exclusive manner and may function independently at different stages of the transport process.

In this study, we did not attempt to identify the kinase that phosphorylates KLC1 at Thr466. The amino acid sequence around Thr466 exhibits some features of a consensus PKC site, and the potential role of PKC will be explored in future work. Interestingly, the phosphorylation level of KLC1 at Thr466 increases in aged mouse brain along with a reduction in JIP1b binding. The elevated phosphorylation of KLC1 at Thr466 that accompanies aging induces a qualitative impairment of APP axonal transport, potentially promoting Aβ generation and contributing to neurodegenerative disorders such as Alzheimer's disease (Stokin *et al.*, 2005; Araki *et al.*, 2007; Vagnoni *et al.*, 2011; reviewed in Brady and Morfini, 2017). Interestingly, okadaic acid (OA) increased the phosphorylation of KLC1 at Thr466. The major target of OA is protein phosphatase 2A (PP2A) which is known to be regulated by various signaling pathways in brain (Ahn *et al.*, 2007; Andrade *et al.*, 2017; Musante *et al.*, 2017). Therefore, KLC1 phosphorylation at Thr466 may also be regulated by PP2A. Moreover, it is well understood that aberrant regulation of PP2A has been implicated in altered phosphorylation of tau, which progresses Alzheimer's disease (AD) pathology (Arif *et al.*, 2014; Wang *et al.*, 2015). Increased phosphorylation of KLC1 at Thr466 may be enhanced in the brain of

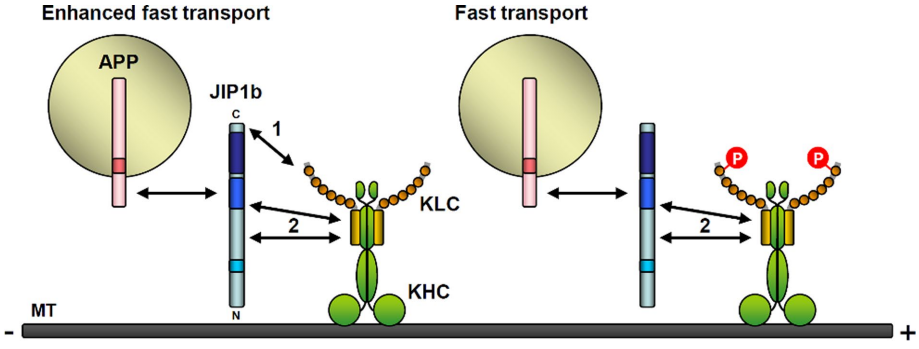


FIGURE 8: Schematic expression of KLC1 phosphorylation at Thr466 on APP cargo transport. Kinesin-1 composed of unphosphorylated KLC1 can associate with JIP1b through the conventional interaction (1) and the novel interaction (2), enabling APP cargoes to be transported efficiently with the enhanced fast velocity (EFV) and the efficient high frequency (EHF) (left). When the kinesin-1 complex contains KLC1 phosphorylated at Thr466 (indicated with P), the conventional interaction (1) between the JIP1 C-terminal region (C11) and the KLC1 TPR region is suppressed, and APP cargoes are transported by the association mediated by the novel interaction alone (2) at the original velocity of kinesin-1 movement (right).

AD patients and cause a further impairment of APP axonal transport in AD brain.

## MATERIALS AND METHODS

### Cell culture and coimmunoprecipitation

African green monkey kidney COS7 cells and mouse neuroblastoma Neuro2a (N2a) cells were cultured as described (Taru *et al.*, 2002). To express proteins or siRNA, COS7 (~$0.8 \times 10^5$) or N2a (~$1.0 \times 10^5$) cells were transiently transfected with the indicated plasmids using Polyethyleneimine MAX (Polysciences) and cultured for 24 h in DMEM containing 10% (vol/vol) fetal bovine serum (FBS). CAD cells, a mouse brain catecholaminergic neuroblastoma cell line, were maintained in DMEM/F12 supplemented with 6% (vol/vol) calf serum (CS) (Qi *et al.*, 1997). Cell lysates were prepared as described (Araki *et al.*, 2007). Lysates and immunoprecipitates were subjected to immunoblot analysis using the indicated antibodies and detected using ECL reagent (GE Healthcare Bio-Sciences, Little Chalfont, UK) or Clarity Western ECL Substrate (Bio-Rad).

Animal studies were conducted in compliance with the guidelines of the Animal Studies Committee of Hokkaido University. All mice were housed in a specific pathogen-free environment in MicroVent units (Allentown).

### In vitro pull-down assay

COS7 cells expressing FLAG-KLC1 were treated with or without 400 nM okadaic acid (OA; Wako Pure Chemical Industries, Osaka, Japan) for 3 h and then lysed with HBS-T buffer (20 mM HEPES pH 7.6, 150 mM NaCl, 0.5% [vol/vol] Triton X-100, 25 µg/ml chymostatin, 25 µg/ml leupeptin, and 25 µg/ml pepstatin). After centrifugation at 20,000 × *g* for 10 min, the supernatants were treated with or without 200 U of λ protein phosphatase (PPase; P9614; Sigma-Aldrich) for 1 h. FLAG-KLC1 was recovered from the lysates by immunoprecipitation with anti-FLAG antibody and Dynabeads Protein G (Thermo Fisher Scientific). To elute FLAG-KLC1 protein, the beads were incubated at 4°C for 30 min in HBS-T containing 0.1 mg/ml FLAG peptide (Sigma-Aldrich). GST and GST-JIP1b$^{351–707}$ were prepared as described (Taru *et al.*, 2002). GST fusion proteins (10 µg) were incubated with 500 ng of FLAG-KLC1 at 4°C for 2 h and then were recovered with glutathione–Sepharose 4B. Input (10 ng protein) and proteins bound to the beads were analyzed by immunoblotting.

### Antibodies

Anti-FLAG (M2; Sigma-Aldrich), anti-HA (12CA5; Sigma-Aldrich), anti-actin (AC-40; Sigma-Aldrich), and anti-JIP1 (B-7; Santa Cruz Biotechnology) antibodies were obtained from the indicated suppliers. Anti-KLC1 (UT109) and anti-KHC (H2) antibodies were described previously (Brady *et al.*, 1990; Araki *et al.*, 2007). Rabbit polyclonal antibody against KLC1 phosphorylated at Thr466 (pThr466) was raised against an antigenic peptide consisting of a Cys residue followed by mouse KLC1$^{462–470}$ containing phosphorylated Thr466 with an amidated C-terminus (C+TVTTpTLKNL-$CONH_2$). The antibody was purified from serum by serial affinity chromatography with the antigen and then by passage through resin conjugated with nonphosphorylated KLC1$^{462–470}$ peptide (C+TVTTTLKNL-$CONH_2$), and a resin conjugated with phosphothreonine (Sigma-Aldrich).

### Phos-tag–based mobility shift assay

FLAG-KLC1 expressed in COS7 cells was recovered by immunoprecipitation with anti-FLAG M2 antibody and separated by Phos-tag SDS–PAGE (Wako Pure Chemical Industries, Osaka, Japan) (Kinoshita *et al.*, 2006). Proteins were transferred onto nitrocellulose membrane following the manufacturer's protocol and probed with anti-FLAG antibody.

### Stoichiometry of KLC1 phosphorylation

N2a cells expressing FLAG-KLC1 were treated with or without okadaic acid (400 nM) for 3 h, and FLAG-KLC1 was recovered by immunoprecipitation with anti-FLAG antibody. The immunoprecipitates were probed with anti-KLC1 (UT109) and anti-pKLC1 antibodies, followed by an ECL-Plus detection system (GE Healthcare Bio-Sciences) and quantitated on a LAS-4000 mini (Fujifilm, Tokyo, Japan). Indicated amounts of KLC1$^{154–172}$ peptide (C+LKKYDDDISPSEDKDSDSS-$CONH_2$) and phosphorylated KLC1$^{462–470}$ peptide (C+TVTTpTLKNL-$CONH_2$) were spotted on nitrocellulose membrane with a Bio-Dot microfiltration apparatus (Bio-Rad), probed with anti-KLC1 (UT109) and anti-pKLC1 antibodies, and quantitated as described above. For each peptide, arbitrary luminescence units were used to draw a standard curve. Amounts of KLC1 and pKLC1 were calculated based on the standard curves, and the ratio of KLC1 phosphorylation was determined.

### ELISA

A 96-well ELISA plate (#9018; Corning) was coated at 4°C overnight with KLC1$^{462–470}$ peptide (C+TVTTTLKNL-$CONH_2$), phosphorylated KLC1$^{462–470}$ peptide (C+TVTTpTLKNL-$CONH_2$), or an unrelated phosphopeptide, APLP2$^{732–740}$ ($NH_2$-DPMLpTPEER+C-$CONH_2$; residue numbers correspond to the APLP2 763 isoform). The wells were washed with PBS and coated with blocking buffer (PBS containing 1% bovine serum albumin (BSA) and 0.05% [vol/vol] Tween-20) for 1 h at room temperature. After removal of the blocking buffer, anti-pKLC1 antibody (0.05 µg IgG) in PBS containing 0.1% BSA and 0.005% (vol/vol) Tween-20 was added, and the plates were incubated at 37°C for 1 h. The wells were washed with PBS, followed by incubation with horseradish peroxidase-conjugated anti-rabbit IgG (GE Healthcare Bio-Sciences, Little Chalfont, UK) at 37°C for 1 h. The plate was washed with PBS, and substrate solution (TMB Microwell Peroxidase Substrate System; Kirkegaard & Perry Lab.) was added to the wells. Following incubation at room temperature for 5 min, stop solution (1 M $H_3PO_4$) was added to the wells, and the absorbance at 415 nm was measured on a microplate reader.

### Total internal reflectance fluorescence microscopy analysis

For imaging, CAD cells were plated at $1 \times 10^4$ cells/well in an eight-well glass-bottom chamber and transfected with Lipofectamine 2000 (Thermo Fisher Scientific) for 10 h. Transfected cells were differentiated by subsequent culture in serum-depleted DMEM/F12 for 48 h. Vesicular transport in processes was observed using a total internal reflectance fluorescence (TIRF) microscopy system (C1; Nikon, Tokyo, Japan) equipped with a CCD camera (Cascade 650; Photometrics). The velocity of anterograde transport was analyzed quantitatively as described (see the Supplemental Information of Araki *et al.*, 2007). Statistical analysis of cargo velocity distributions was performed using the Kruskal–Wallis test followed by Dunn's multiple comparisons test, and average velocities (displayed as histograms) are shown with standard deviations (±SD). The direction of moving vesicles was analyzed by the $\chi^2$ test followed by residual analysis. Cargo vesicles present in the TIRF area, i.e., within ~100 nm of the plasma membrane, were counted using the "count objects" function of Metamorph 6.1 (Molecular Devices). The proportion of anterograde and retrograde vesicles as a percentage of total vesicles, shown as "frequency," was calculated as described (Araki *et al.*, 2007).

Kymographs of moving vesicles in axon and traces of individual vesicles undergoing anterograde transport were assembled using the application Kymomaker (Chiba *et al.*, 2014b; open-access tool at www.pharm.hokudai.ac.jp/shinkei/Kymomaker.html).

### LC-MS/MS analysis

COS7 cells expressing FLAG-KLC1 were treated with 400 nM OA for 3 h and then lysed. FLAG-KLC1 was immunoprecipitated from lysates with anti-FLAG antibody. The immunoprecipitated proteins were resolved by SDS–PAGE, and the bands corresponding to KLC1 were excised and treated with trypsin (Promega). An aliquot (10%) of the digest was directly analyzed with LC-MS/MS. Most of the remainder (80%) of the digest was applied to PHOS-select ion affinity gel (IMAC; Sigma-Aldrich) to enrich for phosphopeptides, and the eluate was dried and reconstituted in 2% acetonitrile/0.1% formic acid for LC-MS/MS analysis in positive-ion mode on an Orbitrap mass spectrometer (Thermo Fisher Scientific). The flow-through fraction from IMAC was subsequently applied to $TiO_2$ resin to enrich it for residual phosphopeptides, and the bound peptides were eluted for LC-MS/MS analysis. Samples were injected into a Waters Symmetry C18 trapping column (300 µm i.d. × 1 cm length), desalted for 5 min at a flow rate of 15 µl/min, and then separated by in-line gradient elution on a 75 µm i.d. × 15 cm Waters BEH C18 column with 1.7 µm particles at a flow rate of 300 nl/min (Waters). Conditions were as follows: linear gradient from 2% to 10% B over 30 s, followed by 10% to 35% B over 60 min, at a flow rate of 300 nl/min; mobile phase A was 0.1% formic acid in water, and mobile phase B was 0.1% formic acid in acetonitrile. The mass spectra were processed by Proteome Discover 1.3, searched against the NCBI nr database using the Mascot searching algorithm (Matrix Science), and finally compiled in Scaffold 3 for data export.

### Immunoprecipitation of endogenous kinesin-1

The cerebrum and cerebellum were dissected from 2- or 22-mo-old mice (C57/BL6) and subjected to homogenization in eight volumes of buffer (20 mM HEPES, pH 7.6, 150 mM NaCl, 0.5% [vol/vol] Triton X-100, 25 µg/ml chymostatin, 25 µg/ml leupeptin, 25 µg/ml pepstatin, 1 mM $Na_3VO_4$, 1 mM NaF, and 1 µM microcystin-LR) followed by centrifugation at 20,000 × *g* for 15 min. After an additional centrifugation at 200,000 × *g* for 30 min, 5 mg protein was incubated with anti-KHC antibody (H2, 5 µg) or the same amount of normal IgG for 12 h. The antibodies were recovered with Dynabeads Protein G (Thermo Fisher Scientific) for analysis.

### Plasmids

Plasmids constructed in vector pcDNA3 or pcDNA3.1, including expression plasmids for JIP1b and KLC1, were described previously (Taru *et al.*, 2002; Araki *et al.*, 2007). Mutant plasmids were prepared by PCR and subcloned into pcDNA3 or pcDNA3.1 (Invitrogen). pcDNA3.1(+)KHC-FLAG was described (Kawano *et al.*, 2012). siRNA against mouse KLC1 and KLC2 were described previously (Araki *et al.*, 2007). siRNA against mouse JIP1b was designed to target nucleotides 1914–1934.

## ACKNOWLEDGMENTS

This work was supported in part by Grants-in-Aid for JSPS Research Fellows (15J02220 to K.C. and 16J04020 to Y.S.); Grants-in-Aid for Scientific Research (15K18854 to S.H., 262930110 and 16K14690 to T.S.) from the Ministry of Education, Culture, Sports, Science and Technology (MEXT) in Japan; National Institutes of Health Grant AG047270 to A.C.N.; the Strategic Research Program for Brain Sciences from the Japan Agency for Medical Research and Development (16dm0107142h0001, 17dm0107142h0002); and a Grant-in-Aid for Scientific Research on Innovative Area-Platforms for Advanced Technologies and Research Resources ("Advanced Bioimaging Support").

## REFERENCES

Ahn JH, Sung JY, McAvoy T, Nishi A, Janssen V, Goris J, Greengard P, Nairn AC (2007). The B"/PR72 subunit mediates Ca2+-dependent dephosphorylation of DARPP-32 by protein phosphatase 2A. Proc Natl Acad Sci USA 104, 9876–9881.

Andrade EC, Musante V, Horiuchi A, Matsuzaki H, Brody AH, Wu T, Greengard P, Taylor JR, Nairn AC (2017). ARPP-16 is a striatal-enriched inhibitor of protein phosphatase 2A regulated by microtubule-associated serine/threonine kinase 3 (Mast 3 kinase). J Neurosci 37, 2709–2722.

Araki Y, Kawano T, Taru H, Saito Y, Wada S, Miyamoto K, Kobayashi H, Ishikawa HO, Ohsugi Y, Yamamoto T, *et al.* (2007). The novel cargo Alcadein induces vesicle association of kinesin-1 motor components and activates axonal transport. EMBO J 26, 1475–1486.

Arif M, Wei J, Zhang Q, Liu F, Basurto-Islas G, Grundke-Iqbal I, Iqbal K (2014). Cytoplasmic retention of protein phosphatase 2A inhibitor 2 (I2PP2A) induces Alzheimer-like abnormal hyperphosphorylation of Tau. J Biol Chem 289, 27677–27691.

Bentley M, Banker G (2016). The cellular mechanisms that maintain neuronal polarity. Nat Rev Neurosci 17, 611–622.

Blasius TL, Cai D, Jih GT, Toret CP, Verhey KJ (2007). Two binding partners cooperate to activate the molecular motor Kinesin-1. J Cell Biol 176, 11–17.

Brady ST, Morfini GA (2017). Regulation of motor proteins, axonal transport deficits and adult-onset neurodegenerative diseases. Neurobiol Dis, doi: 10.1016/j.nbd.2017.04.010.

Brady ST, Pfister KK, Bloom GS (1990). A monoclonal antibody against kinesin inhibits both anterograde and retrograde fast axonal transport in squid axoplasm. Proc Natl Acad Sci USA 87, 1061–1065.

Chiba K, Araseki M, Nozawa K, Furukori K, Araki Y, Matsushima T, Nakaya T, Hata S, Saito Y, Uchida S, *et al.* (2014a). Quantitative analysis of APP axonal transport in neurons—Role of JIP1 in enhanced APP anterograde transport. Mol Biol Cell 25, 3569–3580.

Chiba K, Shimada Y, Kinjo M, Suzuki T, Uchida S (2014b). Simple and direct assembly of kymographs from movies using KYMOMAKER. Traffic 15, 1–11.

Dickens M, Rogers JS, Cavanagh J, Raitano A, Xia Z, Halpern JR, Greenberg ME, Sawyers CL, Davis RJ (1997). A cytoplasmic inhibitor of the JNK signal transduction pathway. Science 277, 693–696.

Fu MM, Holzbaur EL (2013). JIP1 regulates the directionality of APP axonal transport by coordinating kinesin and dynein motors. J Cell Biol 202, 495–508.

Guillaud L, Wong R, Hirokawa N (2008). Disruption of KIF17-Mint1 interaction by CaMKII-dependent phosphorylation: a molecular model of kinesin-cargo release. Nat Cell Biol 10, 19–29.

Hirokawa N, Niwa S, Tanaka Y (2010). Molecular motors in neurons: transport mechanisms and roles in brain function, development, and disease. Neuron 68, 610–638.

Huang Y, Mucke L (2012). Alzheimer mechanisms and therapeutic strategies. Cell 148, 1204–1222.

Huttlin EL, Jedrychowski MP, Elias JE, Goswami T, Rad R, Beausoleil SA, Villen J, Haas W, Sowa ME, Gygi SP (2010). A tissue-specific atlas of mouse protein phosphorylation and expression. Cell 143, 1174–1189.

Kawaguchi K, Ishiwata S (2000). Temperature dependence of force, velocity, and processivity of single kinesin molecules. Biochem Biophys Res Commun 272, 895–899.

Kawano T, Araseki M, Araki Y, Kinjo M, Yamamoto T, Suzuki T (2012). A small peptide sequence is sufficient for initiating kinesin-1 activation through part of TPR region of KLC1. Traffic 13, 834–848.

Kinoshita E, Kinoshita-Kikuta E, Takiyama K, Koike T (2006). Phosphate-binding tag, a new tool to visualize phosphorylated proteins. Mol Cell Proteomics 4, 749–757.

Lu W, Gelfand VI (2017). Moonlighting motors: kinesin, dynein, and cell polarity. Trends Cell Biol, doi: 10.1016/j.tcb.2017.02.005.

Matsuda S, Yasukawa T, Homma Y, Ito Y, Niikura T, Hiraki T, Hirai S, Ohno S, Kita Y, Kawasumi M, *et al.* (2001). c-Jun N-terminal kinase

(JNK)-interacting protein-1b/islet-brain-1 scaffolds Alzheimer's amyloid precursor protein with JNK. J Neurosci 21, 6597–6607.
Meyer D, Liu A, Margolis B (1999). Interaction of c-Jun amino-terminal kinase interacting protein-1 with p190 rhoGEF and its localization in differentiated neurons. J Biol Chem 274, 35113–35118.
Morfini G, Szebenyi G, Elluru R, Ratner N, Brady ST (2002). Glycogen synthase kinase 3 phosphorylates kinesin light chains and negatively regulates kinesin-based motility. EMBO J 21, 281–293.
Musante V, Li L, Kanyo J, Lam TT, Colangelo CM, Cheng SK, Brody AH, Greengard P, Le Novere N, Nairn AC (2017). Reciprocal regulation of ARPP-16 by PKA and MAST3 kinase provides a cAMP-regulated switch in protein phosphatase 2A inhibition. Elife 6, e24998.
Qi Y, Wang JK, McMillian M, Chikaraishi DM (1997). Characterization of a CNS cell line, CAD, in which morphological differentiation is initiated by serum deprivation. J Neurosci 17, 1217–1225.
Scheinfeld MH, Roncarati R, Vito P, Lopez PA, Abdallah M, D'Adamio L (2002). Jun NH2-terminal kinase (JNK) interacting protein 1 (JIP1) binds the cytoplasmic domain of the Alzheimer's beta-amyloid precursor protein (APP). J Biol Chem 277, 3767–3775.
Sobu Y, Furukori K, Chiba K, Nairn AC, Kinjo M, Hata S, Suzuki T (2017). Phosphorylation of multiple sites within an acidic region of Alcadein α is required for kinesin-1 association and Golgi exit of Alcadein α cargo. Mol Biol Cell 28, 3844–3856.
Stockinger W, Brandes C, Fasching D, Hermann M, Gotthardt M, Herz J, Schneider WJ, Nimpf J (2000). The reelin receptor ApoER2 recruits JNK-interacting proteins-1 and -2. J Biol Chem 275, 25625–25632.
Stokin GB, Lillo C, Falzone TL, Brusch RG, Rockenstein E, Mount SL, Raman R, Davies P, Masliah E, Williams DS, Goldstein LS (2005). Axonopathy and transport deficits early in the pathogenesis of Alzheimer's disease. Science 307, 1282–1288.
Suzuki T, Ando K, Isohara T, Oishi M, Lim GS, Satoh Y, Wasco W, Tanzi RE, Nairn AC, Greengard P, *et al.* (1997). Phosphorylation of Alzheimer beta-amyloid precursor-like proteins. Biochemistry 36, 4643–4649.
Suzuki T, Nakaya T (2008). Regulation of amyloid beta-protein precursor by phosphorylation and protein interactions. J Biol Chem 283, 29633–29637.
Taru H, Iijima K, Hase M, Kirino Y, Yagi Y, Suzuki T (2002). Interaction of Alzheimer's beta-amyloid precursor family proteins with scaffold proteins of the JNK signaling cascade. J Biol Chem 277, 20070–20078.
Vagnoni A, Rodriguez L, Manser C, De Vos KJ, Miller CC (2011). Phosphorylation of kinesin light chain 1 at serine 460 modulates binding and trafficking of calsyntenin-1. J Cell Sci 124, 1032–1042.
Vale RD, Reese TS, Sheetz MP (1985). Identification of a novel force-generating protein, kinesin, involved in microtubule-based motility. Cell 42, 39–50.
Verhey KJ, Hammond JW (2009). Traffic control: regulation of kinesin motors. Nat Rev Mol Cell Biol 10, 765–777.
Verhey KJ, Meyer D, Deehan R, Blenis J, Schnapp BJ, Rapoport TA, Margolis B (2001). Cargo of kinesin identified as JIP scaffolding proteins and associated signaling molecules. J Cell Biol 152, 959–970.
Wang X, Blanchard J, Tung YC, Grundke-Iqbal , Iqubal K (2015). Inhibition of protein phosphatase-2A (PP2A) by I1PP2A leads to hyperphosphorylation of Tau, neurodegeneration, and cognitive impairment in rats. J Alzheimers Dis 45, 423–435.
Yip YY, Pernigo S, Sanger A, Xu M, Parsons M, Steiner RA, Dodding MP (2016). The light chains of kinesin-1 are autoinhibited. Proc Natl Acad Sci USA 113, 2418–2423.
Zhu H, Lee HY, Tong Y, Hong BS, Kim KP, Shen Y, Lim KJ, Mackenzie F, Tempel W, Park HW (2012). Crystal structures of the tetratricopeptide repeat domains of kinesin light chains: insight into cargo recognition mechanisms. PLoS One 7, e33943.